Ultra-high *Q* planar silicon microdisk resonators for chip-scale silicon photonics

Mohammad Soltani, Siva Yegnanarayanan and Ali Adibi

School of Electrical and Computer Engineering, Georgia Institute of Technology, 777 Atlantic Drive NW, Atlanta, GA 30332-0250
soltani@ece.gatech.edu

Abstract: We report the fabrication and experimental characterization of an ultra-high *Q* microdisk resonator in a silicon-on-insulator (SOI) platform. We examine the role of the substrate in the performance of such microdisk resonators. While substrate leakage loss has warranted the necessity of substrate undercut structures in the past, we show here that the substrate has a very useful role to play for both passive chip-scale device integration as well as active electronic device integration. Two device architectures for the disk-on-substrate are studied in order to assess the possibility of such an integration of high *Q* resonators and active components. Using an optimized process for fabrication of such a resonator device, we experimentally demonstrate a Q~$3\text{x}10^6$, corresponding to a propagation loss ~0.16 dB/cm. This, to our knowledge, is the maximum *Q* observed for silicon microdisk cavities of this size for disk-on-substrate structures. Critical coupling for a resonance mode with an unloaded Q~$0.7\text{x}10^6$ is observed. We also report a detailed comparison of the obtained experimental resonance spectrum with the theoretical and simulation analysis. The issue of waveguide-cavity coupling is investigated in detail and the conditions necessary for the existence or lack of critical coupling is elaborated.

OCIS codes: (130.3120) Integrated optics devices; (230.5750) Resonators

References and links

1. R. A. Soref and J. P. Lorenzo, "All-Silicon Active and Passive Guided-Wave Components for λ=1.3 and 1.6μm," IEEE J. Quantum Electron. **22,** 873-879 (1986).
2. G. T. Reed and A. P. Knights, *Silicon Photonics: An Introduction*, John Wiley, West Sussex, 2004.
3. L. Pavesi and D. J. Lockwood, *Silicon Photonics*, Springer-verlag, New York, 2004.
4. M. Lipson, "Guiding, Modulating and Emitting Light on Silicon- Challenges and Opportunities," J. Lightwave Technol., **23**, 4222(2005).
5. S. F. Preble, Q. Xu, B. S. Schmidt, and M. Lipson, "Ultrafast all-optical modulation on a silicon chip," Opt. Lett. **30,** 2891–2893 (2005).
6. V. R. Almeida, C. A. Barrios, R. R. Panepucci, and M. Lipson, "All-optical control of light on a silicon chip," Nature **431**, 1081–1084 (2004).
7. A. Liu, R. Jones, L. Liao, D. Samara-Rubio, D. Rubin, O. Cohen, R. Nicolaescu, and M. Paniccia, "A high-speed silicon optical modulator based on a metal-oxide-semiconductor capacitor," Nature **427**, 615–618 (2004).
8. L. Zhou and A. W. Poon, "Silicon electro-optic modulators using p-i-n diodes embedded 10-micron-diameter microdisk resonators," Opt. Express **14**, 6851-6857 (2006).
9. S. J. Emelett and R. A. Soref, "Design and simulation of silicon microring optical routing switches," J. Lightwave Technol., **23,** 1800-1807 (2005).
10. O. Boyraz and B. Jalali, "Demonstration of a silicon Raman laser," Opt. Express **12**, 5269–5273 (2004).
11. H. Rong, R. Jones, A. Liu, O. Cohen, D. Hak, A. Fang, and M. Paniccia, "A continuous-wave Raman silicon laser," Nature **433**, 725–728 (2005).
12. M. Borselli, T. J. Johnson, and O. Painter, "Beyond the Rayleigh scattering limit in high-*Q* silicon microdisks: theory and experiment," Opt. Express **13,** 1515–1530 (2005).

#78962 - $15.00 USD Received 17 Jan 2007; revised 27 Mar 2007; accepted 29 Mar 2007; published 3 Apr 2007

13. M. Borselli, K. Srinivasan, P. E. Barclay, and O. Painter, "Rayleigh scattering, mode coupling, and optical loss in silicon microdisks," Appl. Phys. Lett. **85**, 3693–3695 (2004).
14. T. J. Johnson, M. Borselli, and O. Painter, "Self-induced optical modulation of the transmission through a high-*Q* silicon microdisk resonator," Opt. Express, **14**, 817-831(2006).
15. J. Niehusmann, A. Vörckel, P. H. Bolivar, T. Wahlbrink, W. Henschel, and H. Kurz, "Ultrahigh-quality-factor silicon-on-insulator microring resonator," Opt. Lett., **29**, 2861(2004).
16. P. E. Barclay, K. Srinivasan, O. Painter, B. Lev, and H. Mabuchi "Integration of fiber coupled high-*Q* SiNx microdisks with atom chips", Appl. Phys. Lett., **89,** 131108(2006).
17. A. Yariv, "Universal relations for coupling of optical power between microresonators and dielectric waveguides," Electron. Lett., **36**, 321(2000).
18. M. Cai, O. Painter and K. J. Vahala, "Observation of critical coupling in a fiber taper to silica-microsphere whispering gallery mode system," Phys. Rev. Lett., **85**, 74(2000).
19. D. Weiss, V. Sandoghdar, J. Hare, V. Lef´evre-Seguin, J. Raimond, and S. Haroche, "Splitting of high-*Q* Mie modes induced by light backscattering in silica microspheres," Opt. Lett. **22**, 1835 (1995).
20. B. E. Little, J.-P. Laine, and S. T. Chu, "Surface-Roughness-Induced Contradirectional Coupling in Ring and Disk Resonators," Opt. Lett. **22**, 4–6 (1997).
21. M. L. Gorodetsky, A. Pryamikov, and V. Ilchenko, "Rayleigh scattering in high-*Q* microspheres," J. Opt. Soc. Am. B **17**, 1051–1057 (2000).
22. T. J. Kippenberg, S. M. Spillane, and K. J. Vahala, "Modal coupling in traveling-wave resonators," Opt. Lett. **27**, 1669–1671 (2002).
23. R. J. Hoekstra, M. J. Kushner, V. Sukharev, and P. Schoenborn, "Microtrenching resulting from specular reflection during chlorine etching of silicon," J. Vac. Sci. Technol. B, **16**, 2102 (1998).
24. H. Haus, *Waves and Fields in Optoelectronics*, Prentice-Hall, Englewood Cliffs, New Jersey, 1984.
25. F. Xia, L. Sekaric, and Y. A. Vlasov, "Mode conversion losses in silicon-on-insulator photonic wire based racetrack resonators," Opt. Express, **14**, 3872-3886 (2006).

1. Introduction

Trends toward the integration of micro photonics and microelectronics in a silicon-on-insulator (SOI) platform have had a lot of progress during the recent years [1-4]. The large refractive index of silicon and its low material absorption at telecommunication wavelengths have enabled the realization of a variety of optical functionalities in micron and submicron scales that are compatible with planar CMOS fabrication. In particular, several recent advances include the demonstrations of high-speed silicon (Si) optical modulators [5-8], high-speed switches [7,9], and Si laser sources based on the stimulated Raman effect [10,11]. Among the different micro-photonic components, microdisk and microring resonators have been actively pursued for chip-scale silicon photonics [12-15]. The high quality factors and small mode volumes that are achievable in micrometer scale devices result in very long photon life time and strong electric field enhancement inside these resonators. These unique properties of such microring/microdisk resonators make them ideal candidates for many applications such as filtering, sensing, delay, and enhancement of light-matter interactions [16]. Moreover, since microdisk is a traveling-wave-resonator (TWR), by appropriate design of waveguide-resonator coupling, a complete 100% transmission of energy from a bus waveguide to the resonator is possible [15, 17]. The key challenges in realizing such resonator structures are:

1. Development of improved fabrication techniques in order to reduce surface scattering and absorption loss induced by sidewall roughness in such structures.
2. Engineering of the waveguide-resonator coupling structure to achieve critical coupling.

In this work, we address each of the above challenges in detail and provide guidelines to the design of efficient microdisk resonators suitable for chip-scale photonic integration. We also report the largest *Q*, to our knowledge, which is obtained for such microdisk resonators with integrated input/output coupling structures.

Recently, ultra high *Q* silicon undercut microdisk resonators were demonstrated, and a detailed study of the many of the non-idealities of the high *Q* silicon microdisk structures

#78962 - $15.00 USD Received 17 Jan 2007; revised 27 Mar 2007; accepted 29 Mar 2007; published 3 Apr 2007

including intrinsic material absorption, Rayleigh scattering from surface roughness due to fabrication imperfections, and surface state absorption was presented [12-14]. However, the implementation of microdisk structure in [12-14] was limited to undercut microdisk resonator geometry. In such an undercut microdisk, the SiO_2 layer beneath the Si microdisk is etched resulting in the removal of the silica substrate, and therefore, the microdisk is left isolated from the surrounding. Such undercut microdisk architecture exhibits several challenges in terms of integrating with active electronic functionalities such as metal-oxide-semiconductor (MOS) transistors and p-n junction. Furthermore, the narrow SiO_2 post supporting the undercut microdisk, results in a large thermal resistance from the active microdisk cavity to the Si substrate. Hence, this results in thermal bistability and other unwanted non-ideality as we increase the input optical power impinging on the microdisk cavity. Another challenge with the undercut structures is the difficulty in having a robust and suspended silicon waveguide coupled to the disk. To overcome this problem, in [12-14] silica fiber-taper coupling [18] was employed to couple light from a tapered silica optical fiber to the silicon microdisk. This technique has its own challenges with regards to chip-scale integration, namely: 1) due to the strong phase mismatch between the fiber mode and the Si microdisk mode, energy transfer from the fiber to the microdisk is inefficient, and it is hard to obtain critical coupling; 2) the fiber is suspended and hence it may be sensitive to mechanical vibration as well as damage and degradation due to environmental effects [12].

2. Effect of SiO_2 substrate on the performance of microdisk resonators on SOI substrate

For the goal of integrating several chip-scale functionalities with the microdisk resonator it is essential to use Si-based waveguides for input/output coupling to the microdisk resonator. While undercutting a microdisk resonator is relatively easy, using an undercut waveguide for coupling light to such an undercut resonator is not trivial. For mechanical stability and low-loss performance of the integrated photonic structures it is highly desirable to keep the SiO_2 layer underneath the Si structures intact. In order to assess the impact of the silica substrate, we performed a detailed theoretical study on the effect of oxide substrate on the *Q* of the microdisk resonator. Two structures were considered for this study, namely a conventional SOI microdisk as shown in Fig. 1(a), where the Si layer is completely etched, and a microdisk on Si pedestal as shown in Fig. 1(b), where the Si layer is partially etched and as a result a thin Si pedestal layer is left underneath the microdisk. In the rest of the paper we refer to these two architectures as conventional and pedestal microdisks respectively.

There are two main advantages of the pedestal microdisk, namely the silicon pedestal reduces the thermal resistance of the microdisk and also facilitates its integration with active electronics such as MOS transistors and p-n junctions [5-8,11]. For instance, nonlinear optical applications in silicon suffer from optical power limitations due to two-photon absorption (TPA) generated free carriers [11]. Using the pedestal microdisk architecture, we could potentially integrate a reverse-bias p-n junction with the resonator and sweep the TPA-generated free-carriers away from the microdisk active region [11].

Figure 1 shows the simulation results for the conventional and pedestal microdisk of 20 μm radius. All simulations in this paper have been done using an in-house technique based on the finite element method for the efficient characterization of resonator modes. The code has been implemented using the COMSOL environment to get the benefit of its mathematical library, mesh discretization, and also the graphical user interface (structure definition and field plotting). A perfectly matched layer (PML) absorbing boundary condition was implemented in the code to extract the Q of the resonance modes. For both conventional and pedestal microdisk structures with the radius even as small as 10 μm, the simulations resulted in a radiation $Q>10^{12}$ for a SiO_2 substrate with infinite thickness. Considering the effect of the finite SiO_2 substrate thickness (in the range of 1 μm), a radiation $Q>10^9$ was obtained. Therefore, we conclude that the ultimate limit on the achievable *Q* is limited mostly by the fabrication limitation and other non-idealities in the device and not by the radiation into the

#78962 - $15.00 USD Received 17 Jan 2007; revised 27 Mar 2007; accepted 29 Mar 2007; published 3 Apr 2007

SiO_2 layer. As investigated in [12,14], the major non-idealities are: 1) two-photon absorption assisted free-carrier generation, 2) surface absorption due to the simultaneous presence of sidewall roughness and surface electronic states, and 3) thermal resistance. Thus, our theoretical results suggest that these high *Q*s obtained for undercut microdisk structures [12-14], should be achievable in the microdisk-on-oxide structures (without undercutting). To investigate this observation experimentally, we fabricated a series of microdisk resonators with 20 μm radius on a SOI wafer.

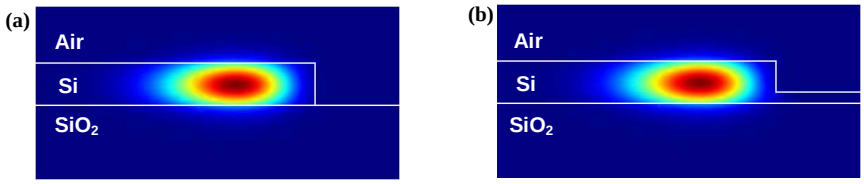

Fig. 1. (a) The cross section of a Si microdisk resonator on oxide substrate, the silicon thickness is 225 nm. (b) The cross section of a pedestal microdisk resonator on oxide substrate; the Si shallow and deep layers have the thicknesses of 60 nm and 225 nm respectively. The energy profile of the fundamental radial TE (electric field predominantly in the plane of the microdisk) mode is shown in the figures. In both cases the disk radius is 20 μm.

3. Fabrication of the structure

By developing a fine etching and fabrication recipe, we were able to fabricate microdisk cavities with smooth sidewalls on SOI. Figure 2 shows the structure of the microdisk resonator coupled to a ridge waveguide. The structure is fabricated on SOITEC SOI with device thickness of 250 nm and buried oxide (BOX) thickness of 3 μm. Fabrication steps starts with growing a 60 nm thermal oxide on SOI wafer as a hardmask. An electron-beam resist ZEP-520A with a thickness of 350 nm is spin coated on the wafer. Then, the structure pattern is transferred onto the wafer using a JEOL-9300 electron-beam-lithography system. Prior works in high *Q* Si microdisks [12] have used the resist reflow process to smooth the microdisk sidewall. In this work, we do not use this process due to the tight resolution requirements for the waveguide-resonator gap, and controlling the sidewall angle in the waveguide and the resonator.

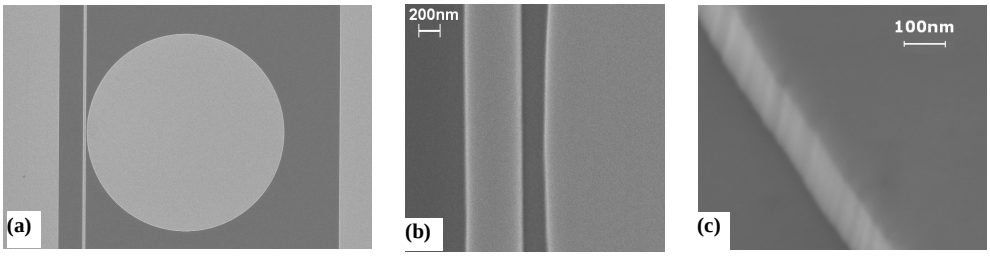

Fig. 2. (a) SEM micrograph of a Si microdisk resonator side-coupled to a waveguide; the disk radius is 20 μm and its thickness is 225 nm. The waveguide width is 550 nm and the gap between the disk and the waveguide is 220 nm. (b) A closer view of the structure at the waveguide-cavity coupling region. (c) Sidewall of the microdisk captured at an azimuth angle 30^o and sample tilt angle 30^o.

In order to define the structure, a two-step etching process is used. The first step is to etch the hard mask with $CF_4/CHF_3/Ar$ gases (3/1/1 ratios) in an inductively coupled plasma (ICP). Then, the resist left on top of the structure is removed and therefore an oxide layer is left on top of the structure as a hardmask. The final step is etching the silicon with Cl_2 in the ICP

#78962 - $15.00 USD Received 17 Jan 2007; revised 27 Mar 2007; accepted 29 Mar 2007; published 3 Apr 2007

chamber. The resulting structure as shown in Fig. 2 is a microdisk with radius of 20 μm, a ridge waveguide with width 550 nm and the gap between the microdisk and the waveguide is 220 nm. The measured sidewall angle was more than 85^{o}. The thickness of the silicon is 225 nm and a thin layer of thermal oxide is left on top of the structure. The effect of this thin thermal oxide on the top of the microdisk may improve the interface properties and consequently the *Q* of the cavity. This issue is under more investigation.

4. Experimental results for the performance of microdisk resonators

4.1. Performance of the conventional microdisk resonators

Figure 3(a) shows the spectrum of the microdisk resonator shown in Fig. 2. The measurement was done using a swept-wavelength test setup. A tunable laser (Agilent Technologies Model 81680A, linewidth 100 kHz), operating in the continuous sweep mode was used as the source. A fiber polarization controller followed by a polarizer was used to control the input polarization state to the device. We used standard objective lens (Newport M-40x, 0.65NA) for coupling into and out of the device. Conventional adiabatic tapering was used at the waveguide input facet in order to reduce the insertion loss. (The waveguide was tapered from 4 μm to 550 nm over a 1 mm length). The output light from the device was spatially filtered using an aperture stop to remove stray light, before being converted to an electrical signal in a photoreceiver (Thorlabs PDB 150C) and interfaced to computer through a data acquisition (DAQ) card (National Instrument PCI-6251, 16-Bit, 1 MS/s). The measured input-output coupling loss was in the range of 20-25dB. The start of each laser wavelength sweep triggered the DAQ card to start data acquisition. Unless otherwise specified, all the measurement results reported in this paper use the TE-polarized light. The laser scan rate was slower than the cavity loading time in order to allow efficient cavity build-up and to obtain meaningful resonance spectrum. During each measurement cycle, the laser was repeatedly scanned several times over the resonant feature to monitor the variations in the resonance spectrum. As can be seen from Fig. 3(a), several different resonant modes with *Q*s ranging from 1.5x10^{5} up to 2.0x10^{6} were observed, corresponding to different radial mode orders.

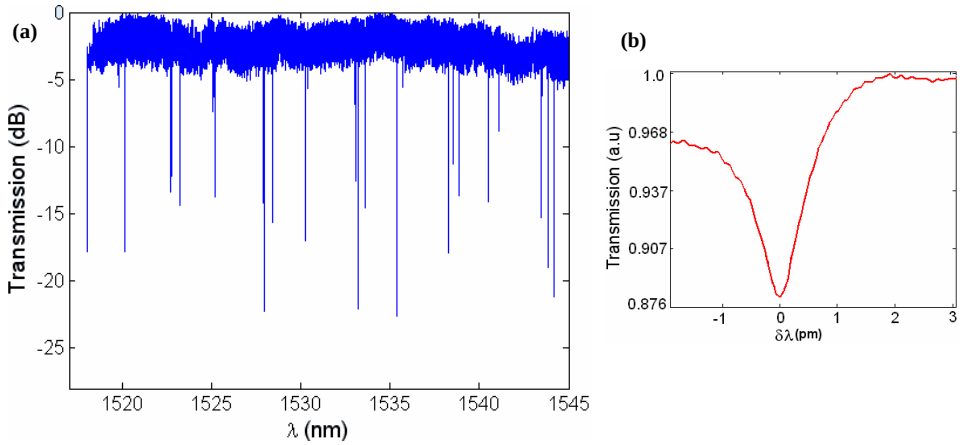

Fig. 3. (a) Spectrum of the microdisk resonator shown in Fig. 2 for TE polarization. (b) An ultra-high *Q*=2x10^{6} was observed at λ=1520.188 nm. From the simulation results, this resonance wavelength corresponds to a 2nd radial order mode with azimuthal number m=218 and an FSR of 5.1 nm. The mode order and FSR are found by comparing the experimental results with the theoretical simulation (which agree very well with the experimental data)

The first few radial mode orders, observed in the experiment, all exhibited a $Q \geq 10^{6}$. Figure 3(b) shows the maximum *Q*~2x10^{6} that was observed. As can be seen from this figure,

#78962 - $15.00 USD Received 17 Jan 2007; revised 27 Mar 2007; accepted 29 Mar 2007; published 3 Apr 2007

due to weak power extinction of this mode, the unloaded Q can be directly obtained by measuring the linewidth of the spectrum. To our knowledge, this is the highest Q reported for a planar silicon microdisk of this radius for conventional disk-on-substrate. The power extinction for each of these resonant modes, shown in Fig. 3(a), varies due to deviations from the critical coupling condition caused by changes in the waveguide-cavity coupling as well as changes in the intrinsic Q of these modes. More details on the conditions necessary to obtain critical coupling are explained in section 5.

One of the issues in the traveling-wave resonators such as microdisk is resonance mode splitting [12, 19-22] resulting from the coupling between degenerate clockwise (CW) and counterclockwise (CCW) traveling wave modes of the resonator due to the sidewall roughness scattering, thereby converting these traveling wave modes into standing wave modes. This mode splitting effect is more pronounced for the modes that have their mode energy concentrated close to the sidewall. The fundamental TE-polarized radial mode of a microdisk has the smallest mode volume and the strongest electric field next to the sidewall and hence exhibits a high sensitivity to the sidewall roughness. Typical observed mode splitting spectrum is shown in Fig. 4. As it can be seen from the figure a splitting of $\Delta\lambda$ = 2.9 pm is observed for this mode which is a quantitative measure of the surface roughness [12]. In our experiments we observed several high Q modes with mode splitting in the range of $\Delta\lambda$ = 2-4 pm.

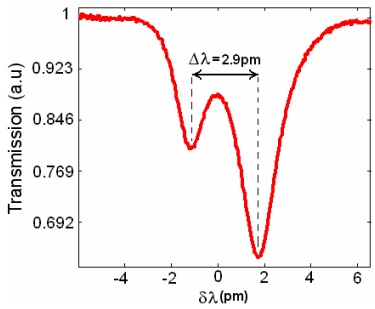

Fig. 4. Observation of resonance mode splitting at resonance λ=1533.642 nm for the microdisk shown in Fig. 2.

4.2 Performance of the pedestal microdisk resonators

Pedestal microdisks, such as the one shown in Fig. 1(b), were also fabricated and characterized. The disk radius and the input/output coupling waveguide are identical to the microdisk shown in Fig. 2, with the only difference being that by controlling the etching depth of the microdisk, we leave a thin pedestal layer of silicon under the resonator. FEM simulations show that the radiation Q of this structure is very large ($Q > 10^{12}$). Hence, we anticipate that the Q is limited only by the fabrication imperfections, surface roughness, and other non-idealities. Figure 5 shows the SEM cross section of this device. From the SEM measurement, the thickness of the thin pedestal layer, after the fabrication, was in the range 63 nm ± 3 nm. As can be seen from this figure, trenching is observed at the interface of the device and the pedestal layer. This trench formation, which is typical in Cl_2 chemistry based plasma etching of silicon [23], can be further reduced by more optimization of the Si etch recipe.

Figure 6(a) shows the spectrum of this pedestal microdisk. From this figure, we observe that the spectrum exhibits less resonance features compared to the resonance spectrum of the conventional microdisk as shown in Fig. 3(a). Based on the comparison between the numerical simulation and experimental observation of resonance locations, most of the

#78962 - $15.00 USD Received 17 Jan 2007; revised 27 Mar 2007; accepted 29 Mar 2007; published 3 Apr 2007

disappearing resonance features in pedestal microdisk belong to very high order radial modes, while the first few order radial modes still exhibit high *Q*s. A qualitative explanation for this increased loss for higher order modes can be obtained as follows: Due to the traveling wave nature of the whispering gallery modes, an effective mode index of propagation can be specified for each mode. Generally, the higher order modes of any dielectric guiding structure, (e.g. disk) have a lower effective index, hence a lower phase-mismatch to the leaky and radiation modes. This results in a stronger coupling of these higher order modes to the radiation and leaky modes due to the presence of surface roughness. Therefore, for the case of the pedestal microdisk, the higher radial order modes of the disk have stronger coupling to the leaky modes of this Si slab pedestal layer. Increasing the thickness of the Si pedestal layer results in an even higher coupling to the leaky modes of this slab layer, and this results in a dramatic reduction in the *Q* of the disk higher radial order modes.

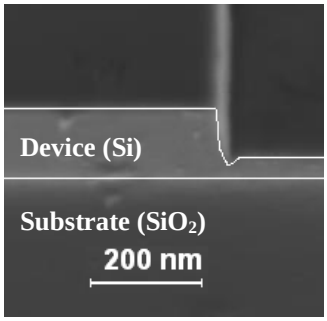

Fig. 5. SEM cross section of the pedestal type structure captured at a sample tilt angle of 30°. The microdisk radius and thickness are 20 μm and 225 nm respectively, and the thickness of the shallow pedestal layer is 65 nm.

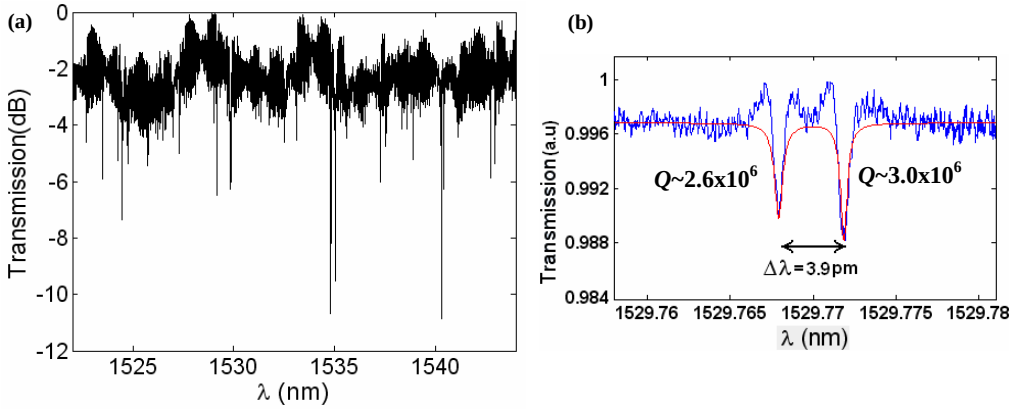

Fig. 6. (a) Spectrum of the pedestal microdisk resonator coupled to a waveguide for TE polarization. (b) Spectrum of the 2nd order radial mode; mode-splitting due to the coupling of CW and CCW is observed. The theoretical Lorentzian spectrum, which is shown as the solid red curve in Fig. 6(b), resulted in unloaded *Q*s in agreement with the experimental *Q*s. The disk radius and the input/output coupling waveguide are identical to the conventional microdisk shown in Fig. 2.

Figure 6(b) shows the resonance spectrum of the 2nd order radial mode. As it can be seen from this figure, resonance splitting is observed for this mode and the power extinction in the spectrum is very weak. Therefore the cavity is almost unloaded and by measuring the

#78962 - $15.00 USD Received 17 Jan 2007; revised 27 Mar 2007; accepted 29 Mar 2007; published 3 Apr 2007

linewidth of the spectrum the unloaded Q was simply estimated to be about $3.0\text{x}10^6$ in this pedestal microdisk architecture. This Q corresponds to a propagation loss α~0.16 dB/cm. This, to our knowledge, is the highest recorded Q for a pedestal microdisk cavity on substrate. To confirm these experimental results, a conventional coupled mode theory including the effect of mode splitting was employed. This theoretical Lorentzian spectrum, which is shown as the solid red curve in Fig. 6(b), resulted in unloaded Qs in agreement with the experimental Qs. We anticipate this pedestal microdisk to be an enabling device platform suitable for integration with p-n junctions and other active electronic components with great potential to be used for modulation and switching applications.

5. Engineering the waveguide-cavity coupling for efficient energy transfer

In the course of our experiments with the conventional and pedestal microdisk, we noticed that while several of the higher radial order modes exhibited critical coupling, for the first few order modes, which are of significant interest due to their high Q and low mode volume, we were unable to obtain critical coupling. In order to look into this issue more closely, we employed a coupled-mode theory formalism to study the waveguide-cavity coupling [24].

Figure 7(a) shows the structure of a TWR coupled to a waveguide. In such TWR-waveguide structures, in the weak coupling regime, the power transmission and the total loaded quality factor (Q_L) at resonance are respectively expressed as:

$$T(\omega_0) = \frac{P_{out}}{P_{in}} = \left| \frac{1 - Q_0 / Q_c}{1 + Q_0 / Q_c} \right|^2 \tag{1}$$

$$Q_L^{-1} = Q_0^{-1} + Q_c^{-1} \tag{2}$$

In the above expression Q_0 and Q_c are respectively the intrinsic quality factor and coupling quality factor, with the coupling quality factor (Q_c) being used as a measure of rate of energy decay from the cavity to the waveguide, i.e. stronger coupling between the waveguide and the cavity results in smaller Q_c. As it can be seen from Eq. (1), in order to completely transfer energy from waveguide to the resonator at the resonance, Q_0 and Q_c should be equal and as a result Q_L becomes half of Q_0. This condition is also referred to as critical coupling [17]. From Eq. (1) and (2), by changing Q_c, both Q_L and the power transmission through the waveguide change as shown in Fig. 7(b). Therefore, it is crucial to adjust Q_c to obtain the required Q_L and power transfer to the cavity.

In a TWR-waveguide coupling structure, Q_c depends on the cavity mode volume, coupling interaction length, and effective mode index matching between the waveguide and TWR modes. Larger cavity mode volumes increase Q_c, while larger coupling interaction lengths result in reduction of Q_c. However, the effect of the mode index mismatch between the disk and the waveguide on Q_c is dramatic, and is illustrated below. Since the microdisk resonator is a TWR structure, as shown in Fig. 7(a), we can ascribe to each microdisk mode, a phase and an associated effective mode index. In the case of the large index mismatch between the microdisk and the waveguide, coupling is strongly reduced, so much so that even bringing the waveguide very close to the cavity does not significantly alter their coupling. Moreover, putting the waveguide and resonator too close to each other results in strong perturbation of the cavity structure [25], resulting in additional loss and the resultant degradation of the Q. In order to illustrate this coupling and index matching issue, using the coupled mode analysis, we consider the microdisk and waveguide whose dimensions are given in Fig. 2.

Figure 8(a) shows the effective mode index for different radial modes of this microdisk. The effective index of the fundamental TE mode of the waveguide is also shown in this figure. As it can be seen, the 3rd order radial microdisk mode has an effective index that is closer to that of the waveguide. Hence, we expect this mode to be better phase matched to the

#78962 - $15.00 USD Received 17 Jan 2007; revised 27 Mar 2007; accepted 29 Mar 2007; published 3 Apr 2007

waveguide mode, thereby resulting in a strong coupling. Figure 8(b) shows the calculated coupling Q (Q_c) for different waveguide-cavity gaps, based on a coupled-mode formalism and using the FEM calculated field profiles for the disk and waveguide. As it can be seen from Fig. 8(b), the 3rd order radial mode has a lower value of Q_c, thereby confirming the prediction of better waveguide-cavity coupling, i.e. closer to critical coupling, than the lower order modes based on the phase-mismatch obtained from effective indices in Fig. 8(a). For a gap of 220 nm, for the 1st order radial mode, Q_c was calculated to be $40\text{x}10^6$. Therefore, it is reasonable not to be critically coupled to the fundamental mode for these waveguide-resonator geometry parameters. The same argument applies for the 2nd and 3rd order modes. However, for the gap of 150 nm, the values of Q_c vary in the range of $1\text{x}10^6$-$10\text{x}10^6$ and are closer to what we may achieve for the intrinsic Q of the cavity, thereby ensuring we are closer to critical coupling.

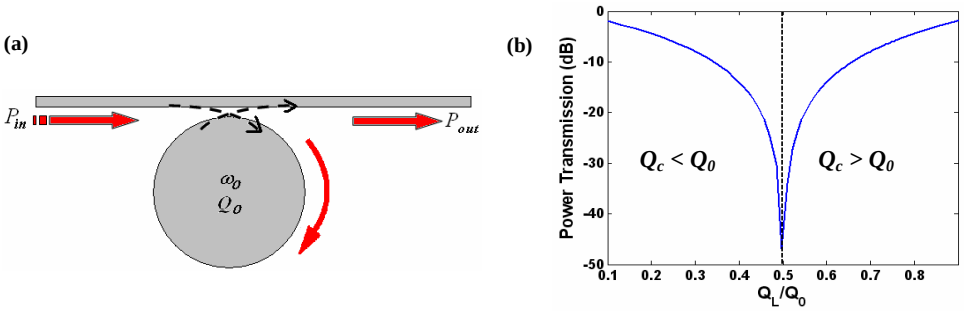

Fig. 7. (a) Graphical representation of the coupling between a waveguide and a microdisk resonator. (b) Power transmission through the waveguide versus normalized loaded quality factor (Q_L/Q_0).

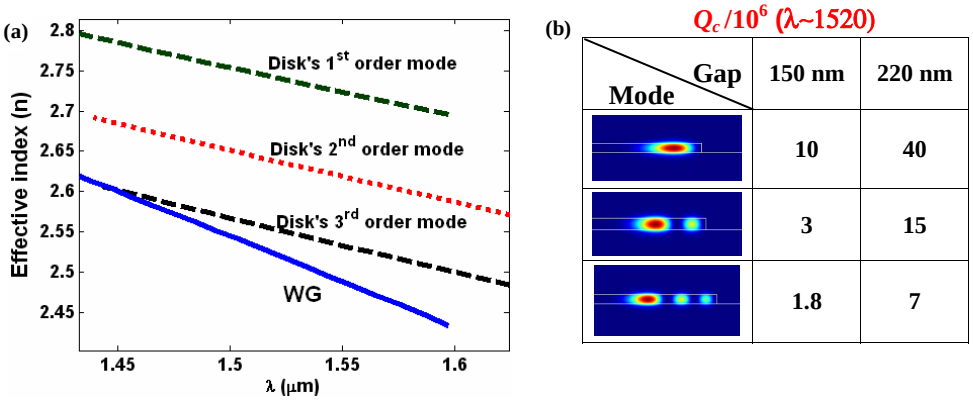

Fig. 8. (a) Comparison of the effective indices of the traveling TE modes of the microdisk resonator shown in Fig. 2 for different radial mode orders with that for the waveguide. The dimension of the disk radius and the waveguide is given in the caption of Fig. 2. (b) Q_c for different gaps between the waveguide and the microdisk calculated using coupled mode theory

To validate these coupling studies, we considered a microdisk with a radius of 10 μm. Figure 9(a) shows the effective indices of the microdisk TE modes and the fundamental waveguide TE mode. From this figure, it can be seen that the 2nd radial mode of the microdisk is better index-matched to the waveguide mode. Therefore, this mode is expected to have stronger coupling as compared with the 1st and 3rd order modes. The table shown in Fig. 9(b)

#78962 - $15.00 USD Received 17 Jan 2007; revised 27 Mar 2007; accepted 29 Mar 2007; published 3 Apr 2007

shows the results of the calculation for Q_c for the gaps of 150 nm and 220 nm. It is clearly seen from Fig. 9(b) that the lowest Q_c, i.e. the strongest coupling, is obtained for the 2nd radial order cavity mode for both 150 nm and 220 nm waveguide-cavity gaps. This agrees very well with the phase-matching obtained for the 2nd order mode as shown in Fig. 9(a). In addition, reducing the size of the microdisk results in a smaller mode volume. Therefore, the magnitude of the disk electric field increases near the waveguide which results in a stronger interaction between the disk mode and the waveguide mode and consequently reduces Q_c. Furthermore, the intrinsic Q value of about $1x10^6$-$5x10^6$ are achievable for the 2nd radial order mode of the microdisk with practical fabrication techniques, suggesting the possibility of obtaining critical coupling for the 2nd order mode of the microdisk resonator. Also, note that the coupling of the waveguide and the 1st order mode of the resonator is strong (i.e. same order as that of the 2nd mode). By further reduction of the disk size, we can achieve a better phase matching to the 1st order resonator mode with practical coupling parameters to 550nm waveguide. This is very important for practical applications due to the small mode volume of the 1st order mode of the disk.

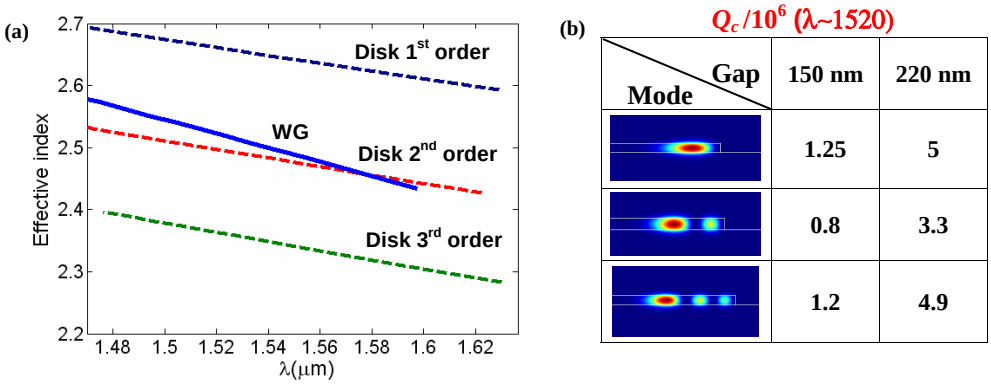

Fig. 9. (a) Comparison of the effective indices of the traveling TE modes of the microdisk resonator with radius of 10μm with that for the waveguide. The dimensions of the waveguide are given in the caption of Fig. 2. (b) Q_c for different gaps between the waveguide and the microdisk.

The results shown in Fig. 8 and Fig. 9 clearly demonstrate the importance of the phase-matching of the waveguide and the cavity modes for achieving good coupling. This fact was experimentally confirmed by achieving critical coupling for the 4th order radial mode which is closely index matched to the waveguide, as shown in Fig. 10. As it can be seen in this figure, almost 99% of the energy is transferred from the waveguide to the cavity at resonance. From this spectrum an unloaded Q~$0.7x10^6$ was extracted. This, to our knowledge, is the most efficient waveguide-microdisk critical coupling to the highest cavity Q that has been demonstrated in an integrated planar silicon photonics platform.

Hence, in summary, in order to obtain critical coupling, the mode index dispersion of the waveguide and the microdisk should be engineered in order to first achieve the phase matching between the waveguide mode and the desired cavity mode, with more emphasis placed on optimizing the disk dimensions. This mode dispersion engineering is then followed by a fine tuning of the gap spacing between the waveguide and the disk to obtain the desired range of Q_c for critical coupling to the desired microdisk radial mode order and at the desired wavelength range. Efforts for experimental demonstration of such optimally engineered critical coupling for the lower radial order high Q modes are currently underway.

#78962 - $15.00 USD Received 17 Jan 2007; revised 27 Mar 2007; accepted 29 Mar 2007; published 3 Apr 2007

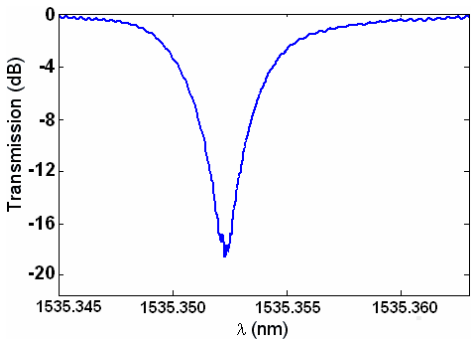

Fig. 10. (a) Experimental observation of critical coupling for the 4th order radial mode of the conventional microdisk shown in Fig. 2. The coupling of about 99% of the power into the cavity is clear. Also, the measured unloaded *Q* is about 0.7×10^6.

6. Summary

In summary, we have demonstrated ultra-high *Q* planar microdisk resonators on SOI platform without any undercutting. It was shown that the presence of the substrate while not limiting the *Q*, instead offers the potential for significant device benefits in terms of enabling chip-scale integration of active components and also in terms of improving the heat sink. Two architectures for the disk-on-substrate were considered: 1) conventional disk, 2) pedestal microdisk. For the conventional microdisk on substrate a $Q \sim 2.0 \times 10^6$ was measured. For the pedestal-type microdisk a $Q \sim 3.0 \times 10^6$ was measured. These are the highest *Q*'s reported for a Si microdisk-on-substrate with similar dimensions. Critical coupling with almost 99% energy transfer from the waveguide to the microdisk was experimentally observed for the 4th radial order mode with an unloaded $Q \sim 0.7 \times 10^6$. Using a theoretical formalism based on the coupled-mode approach, the microdisk-waveguide coupling was investigated in detail. The reason for the lack of critical coupling of the first few radial order modes in our experimental results was clearly explained. This coupling analysis was used to propose a systematic method for engineering the modal dispersion of the waveguide and the microdisk, in order to obtain critical coupling to the desired microdisk radial mode at the desired operating wavelength.

Acknowledgments

This work was supported by Air Force Office of Scientific Research under Contract No. FA9550-06-01-2003 (G. Pomrenke). The authors would like to thank Dr. J. D. Huang, B. Momeni, Dr. M. Borselli, and Dr. S. Spillane for useful discussions.

#78962 - $15.00 USD Received 17 Jan 2007; revised 27 Mar 2007; accepted 29 Mar 2007; published 3 Apr 2007